Energy Proceedings
Vol 50, 2025
ISSN 2004-2965

A GIS-based Co-Planning Approach for District Heating Networks[#]

Jonathan Vieth[1], Jan Westphal[1], Arne Speerforck[1]

1 Hamburg University of Technology, Institute of Engineering Thermodynamics

(Corresponding Author: jonathan.vieth@tuhh.de)

ABSTRACT

District heating networks (DHNs) play a vital role in the transition of the heating supply of buildings to renewable sources. The sizing of the pipes of the DHN and the temperatures within the DHN each affect the heat losses and the required pumping power. In addition, the efficiency of a heat pump supplying the DHN is affected as well. Therefore, a *co-planning* approach that includes the operation of the DHN in the planning is required. This paper presents a co-planning approach based on real GIS data. The approach uses only five design variables (two for dimensioning the pipes, two for the supply temperature, and one for the producer). The optimal design variable configuration is determined by an optimization algorithm. The optimization includes a full year simulation of the DHN. The result of the planning process is a fully parameterized DHN with a matching supply temperature.

Keywords: district heating network simulation, district heating network planning, graph theory, co-planning

NONMENCLATURE

Abbreviations	
GIS	geographic information system
DHN	district heating network
LSHP	large-scale heat pump
TPL	target pressure loss
OSM	Open Street Map
CHP	combined heat and power unit
COP	coefficient of performance
Symbols	
z	design variable
J	objective function
y	expansion planning variable
u	operational planning variable
x	geographic coordinate
T	temperature in °C
Q	heat energy in J
$\dot{Q}$	heat flow in W
G	graph
E	set of edges
V	set of vertices
o	origin of edge
t	tail of edge
f	distance function
H	set of houses
v	vertex
ζ	loss coefficient
l	length in m
d	diameter in m
U	heat loss factor in W/mK
$\dot{m}$	mass flow in kg/s
c_{w}	heat capacity of water in J/kg K
ρ	density of water in kg/m^3
λ	friction factor
ϵ	wall roughness in m
Re	Reynolds number
μ	dynamic viscosity in Pa s
p	pressure in Pa
η	efficiency factor
P	power in W
COP	coefficient of performance
Δt	time-span of a time-step in s
K	set of time-steps
c	cost
σ	debt and equity ratio
r	interest rate
w	lifetime in a
C	effective thermal capacity in Wh/K
$\mathrm{c}_{\mathrm{eff}}$	specific effective thermal capacity in Wh/m^{2}K
A	net building area in m^2
G	thermal conductivity in W/K
η_{C0}	Carnot efficiency factor
E	energy in J
γ	energy losses in %
Δ	difference

This is a paper for the 16th International Conference on Applied Energy (ICAE2024), Sep. 1-5, 2024, Niigata, Japan.

Subscripts	
S	supply
R	return
OSM	Open Street Map
air	air
soil	soil
set	set
TOP	topology of the DHN
H	houses
P	producer
L	closest connection of point with edge
LC	largest graph component
A	all possible routing options
$*$	optimum
SIM	simulation
max	maximum
min	minimum
pu	pump
pi	pipe
LSHP	large-scale heat pump
CHP	combined heat and power unit
el	electric
gas	gas
gtp	gas to power
gth	gas to heat
fuel	fuel
inv	investment
equity	equity
debt	debt
C	critical consumer

1. INTRODUCTION

In order for Germany to fulfill the goals of the European Green Deal, the heat supply of buildings has to be decarbonized by 2050 [1]. A recent study revealed that the share of buildings supplied by DHNs with heat must increase in order to fulfill the goals [2]. The study analyzed four scenarios. In three out of four scenarios the share of houses connected to DHNs in 2045 is at least double that in 2020.

However, in order for a DHN to supply houses with carbon-neutral heat, the technologies feeding heat into the DHN must undergo a transformation. One technology that has been the subject of much discussion is large-scale heat pumps (LSHPs) [3]. The efficiency of LSHPs depends on the supply temperature, i.e. on the operation of the DHN. Hence, the planning of a DHN supplied by at least one LSHP must incorporate the operation of the DHN into the planning process. This integration of operation into energy system planning is referred to as *co-planning* [4]. [5] analyzed the impact of DHN pipe sizing on heat and pressure losses. In order to describe the sizing of the pipes with one parameter, the term *target pressure loss* (TPL) was introduced. The TPL describes the pressure losses per unit length in the DHN.

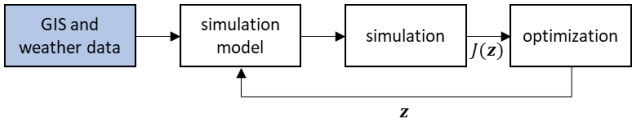

Fig. 1 Procedure of the co-planning approach.

In this work, we introduce a co-planning approach for DHNs. The general procedure is depicted in Fig. 1. The approach uses real-world geographic information system (GIS) data to identify the optimal DHN topology. In a second step, the topology is parameterized based on a TPL for the supply pipes and a TPL for the return pipes. Supply pipes in DHNs often have a smaller diameter than the associated return pipes, due to the higher temperatures in supply pipes. The result of the parameterization is a simulation model in the modeling language *Modelica*. The generation of the simulation model from GIS data is described in Section 2. The simulation model is part of an optimization. The optimizer influences the vector of design variables $\boldsymbol{z} = [\boldsymbol{y} \quad \boldsymbol{u}]$ for minimizing the total cost $J(\boldsymbol{z})$ of the DHN, where $\boldsymbol{y} = [y_\mathrm{S} \quad y_\mathrm{R} \quad y_\mathrm{P}]$ are the extension planning variables and $\boldsymbol{u} = [u_0 \quad u_1]$ are the operational planning variables. The design variables are the TPL of the supply pipes (y_S), of the return pipes (y_R), two parameters u_0 and u_1 of the supply temperature, as discussed in more detail in Section 2.6, and a parameter y_P for finding the optimal producer type. Section 3 provides a more detailed description of the optimization process. In Section 4, a case study is presented. The presented co-planning approach is used for finding the optimal DHN for the case study. In Section 5, the results of the case study and the co-planning approach are discussed.

Notation. A graph $G = (V, E)$ is a tuple with the set of vertices V and the set of edges E. All graphs considered in this work have no parallel edges and no loops. The origin of each edge $e \in E$ is denoted by $o(e) \in V$ and the tail by $t(e) \in V$ [6]. Each vertex $v \in V$ has a horizontal $x_1(v)$ and vertical $x_2(v)$ geographic coordinate.

2. MODEL GENERATION

The optimization approach presented in Fig. 1 requires the automated generation of a simulation model based on GIS and weather data and $\boldsymbol{z}$. The automated model generation is described in this section. The overall procedure is depicted in Fig. 2.

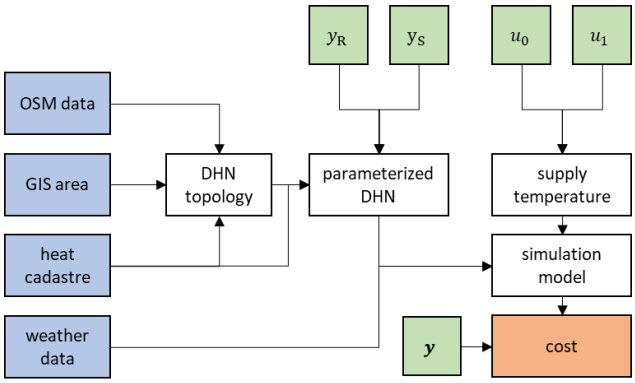

Fig. 2 Procedure of generating the simulation model. Inputs in blue, outputs in red, and design variables of the optimization in green.

2.1 Input Data

As illustrated in Fig. 2, the co-planning approach presented necessitates inputs comprising a heat cadastre, open street map (OSM) data, and weather data for one representative year. The heat cadaster used is based on [7]. For each house h, that is part of the heat cadastre, following data must be provided: the location $x_1(h)$ and $x_2(h)$, the yearly heating demand Q_h for the representative year, and a maximum required heating power $\dot{Q}^h_{\max}$. The required weather data is the air temperature T_{air} and the soil temperature T_{soil}.

2.2 Network generation

Given the extensive availability of GIS and graph theory packages, the programming language *Python* is employed for network generation. First, the OSM data is loaded and cropped to the area of interest using the *OSMnx* package [8]. The result is a *distance graph* $G_{\text{OSM}} = (V_{\text{OSM}}, E_{\text{OSM}}, f_{\text{OSM}})$ with the set of vertices V_{OSM} and the set of edges E_{OSM} of the street network. The mapping $f_{\text{OSM}}: E_{\text{OSM}} \to \mathbb{R}_{\geq 0}$ maps the edges to their matching distances. A distance may be any value related to the cost of constructing the pipe represented by the edge e. However, we assume that the distance of edge e is the geographic distance between $o(e)$ and $t(e)$. For a definition of *distance graphs* see [9]. Next, a set of houses H is selected from the houses within the specified area of interest. A vertex v_{P} is chosen as the location for the producer.

The DHN topology is derived through a series of steps. First, in order to connect house or producer $i \in H \cup \{v_{\text{P}}\}$ with G_{OSM}, the closest vertex v_i of G_{OSM} is selected and connected by an edge $e = (v_i, i)$ with i. The vertex v_i may be a vertex $v \in V_{\text{OSM}}$ or any point that is located on one of the edges $e \in E_{\text{OSM}}$. This step results in the distance graph $G_{\text{H}} = (V_{\text{H}}, E_{\text{H}}, f_{\text{H}})$ with

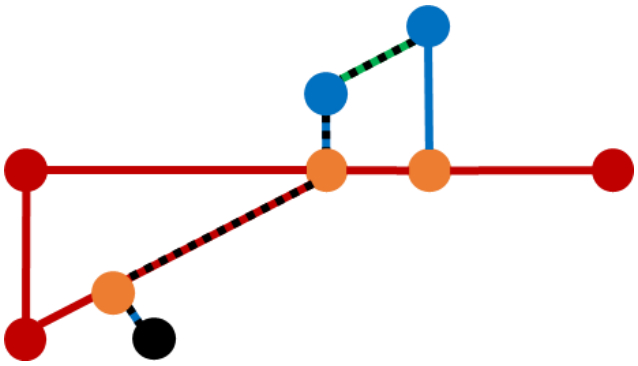

Fig. 3 Example of finding the optimal DHN topology. G_{OSM} in red, H in blue, p_{P} in black, V_{L} in orange, E_{H} in red and blue, E_{A} in red, blue, and green, E^* is depicted by black dashed lines.

$V_{\text{H}} = V_{\text{OSM}} \cup V_{\text{L}} \cup H \cup \{v_{\text{P}}\}$, where $V_{\text{L}} = \{p_i | \forall i \in H \cup \{v_{\text{P}}\}\}$.

Since cropping the OSM data to the area of interest might lead to a dissected street network, G_{H} might consist of several components. Hence, the largest graph component $G_{\text{LC}} = (V_{\text{LC}}, E_{\text{LC}}, f_{\text{LC}})$ is selected. To account for the possibility of houses being located in a second row, each $h \in H$ is connected with the closest houses by edges. This procedure results in the distance graph $G_{\text{A}} = (V_{\text{A}}, E_{\text{A}}, f_{\text{A}})$ describing all possible routing options for finding the optimal DHN topology.

Next, the optimal DHN topology $G^* = (V^*, E^*)$ has to be found based on G_{A}. Optimality is defined with regard to an objective function

$$J_{\text{TOP}}(E_{\text{A}}) = \sum_{e \in E_{\text{A}}} f_{\text{A}}(e). \qquad (1)$$

The purpose of a DHN is to connect all houses with the heat generating unit. Therefore, it is required that the houses and the location of the producer v_{P} are a part of V^*, i.e. $H \cup \{v_{\text{P}}\} \in V^*$. The graph G^* is a *Steiner Tree*. For a definition of *Steiner Trees* see [10]. In this work, the algorithm presented in [9] is used implemented in the Python package *NetworkX* [11] for solving the optimization problem (1). An Example of finding G^* from G_{OSM}, v_{P}, and H is depicted in Fig. 3.

2.3 DHN parameterization

This section deals with deriving a simulation model $G_{\text{SIM}} = (V_{\text{SIM}}, E_{\text{SIM}})$ for the DHN based on G^*. Since a DHN consists of a supply and a return line, for each edge $e \in E^*$ two edges $s \in E_{\text{S}}$, $r \in E_{\text{R}}$ exist with $E_S, E_R \subset E_{\text{SIM}}$. Furthermore, houses and producers are modeled by edges linking the supply line with the return line. For each $e \in E_{\text{SIM}}$ parameters need to be calculated in order to be able to simulate the DHN. For each house

$h \in E_{\mathrm{H}}$ a loss coefficient $\zeta_h = \zeta = 5$ is assumed. For each pipe $p \in E_{\mathrm{S}} \cup E_{\mathrm{R}}$ a length l_p, a diameter d_p, a pipe roughness ϵ_p, and a heat loss factor U_p have to be known. The length l_p is known due to the distance of $o(p)$ to $t(p)$ and $\epsilon_p = \epsilon = 0.07\,\mathrm{mm}$ is assumed to be constant over all pipes. Assuming a constant temperature difference $\Delta T = T_{\mathrm{S}} - T_{\mathrm{R}} = 30\,°\mathrm{C}$ with the supply temperature T_{S} and the return temperature T_{R} for each house $h \in E_{\mathrm{H}}$ a maximum required mass flow $\dot{m}^h_{\max} = \frac{\dot{Q}^h_{\max}}{c_{\mathrm{w}} \Delta T}$ can be calculated with the constant heat capacity of water $c_{\mathrm{w}} = 4183\,\mathrm{J/kgK}$. Since G^* is a tree, for each pipe $p \in E_{\mathrm{S}} \cup E_{\mathrm{R}}$ a mass flow $\dot{m}^p_{\max}$ follows directly from $\dot{m}^h_{\max}$.

As shown in Fig. 2, the supply TPL y_{S} and the return TPL y_{R} are design variables of the model generation. Hence, the maximum pressure loss in pipe $p \in E_i$ is

$$\Delta p^p_{\max} = l_p y_i \tag{2}$$

for $i \in \{\mathrm{S}, \mathrm{R}\}$. The mass-flow-pressure-loss-correlation

$$\Delta p_p = \frac{8 l_p \lambda(\dot{m}_p)}{\pi^2 \rho d_p^5} \dot{m}_p^2 \tag{3}$$

with the constant water density $\rho = 983.19\,\mathrm{kg/m^3}$ and the friction factor correlation [12]

$$\lambda(\dot{m}_p) = \left[-2 \log\left(2.7 \frac{\log\left(\mathrm{Re}(\dot{m}_p)\right)^{1.2}}{\mathrm{Re}(\dot{m}_p)} + \frac{\epsilon_p}{3.71 d_p} \right) \right]^{-2} \tag{4}$$

by Zanke for turbulent flows can be used for linking $\dot{m}^p_{\max}$ with $\Delta p^p_{\max}$. The Reynolds number is given by

$$\mathrm{Re}(\dot{m}_p) = \frac{4}{\pi \mu d_p} \dot{m}_p \tag{5}$$

with the constant dynamic viscosity $\mu = 466 \cdot 10^{-6}\,\mathrm{kg/m\,s}$. For each pipe $p \in E_i$ with $i \in \{\mathrm{S}, \mathrm{R}\}$ a diameter d_p can be calculated by solving the nonlinear system of equations $(2) - (5)$. Afterwards, out of a catalogue of possible diameters, the closest diameter to d_p has to be chosen. For each pipe p, contained in the catalogue, a matching U_p has to be available.

2.4 Simulation model

Since no Python tool exists for dynamic DHN simulations, the DHN is simulated in Modelica using Dymola. In the following, the governing equations used are described. For all equations, static fluid parameters ρ, μ, and c_{w} are assumed.

2.4.1 Pipes

Most of the components used in this study are based on the three balance equations of energy, mass, and momentum. The mass and the momentum balance are assumed to be static. The energy balance is considered dynamic to allow an investigation of thermal inertia. It is discretized using the upwind scheme for the enthalpy flows, comparable to the approach in [13]. For each pipe p, heat losses are considered by U_p. For the momentum balance, a pressure loss model for a straight pipe from the FluidDissipation library [14] is used. It is based on the Darcy-Weissbach equation and considers different flow regimes.

2.4.2 Junctions

Similar to the pipe model, the junction model contains a static mass and momentum balance. A lumped control volume is used for the energy balance of the junctions. Heat losses are not considered, and a linear pressure loss model is assumed.

2.4.3 Houses

The consumer model consists of a pump, a heat exchanger, a P-controller, and the house itself. Each house h is modelled by a thermal capacity $C_h = c_{\mathrm{eff}} A_h$ with the effective heat capacity $c_{\mathrm{eff}} = 90\ \mathrm{Wh/m^2K}$ and the net building area A_h [15] and a thermal conductivity

$$G_h = \frac{Q_h}{24\mathrm{h} \sum_{d=1}^{365} \begin{cases} T_{\mathrm{set}} - T_{\mathrm{air}}(d), & T_{\mathrm{air}}(d) \le 16°\mathrm{C}, \\ 0, & \text{otherwise} \end{cases}}$$

with the set temperature $T_{\mathrm{set}} = 21°\mathrm{C}$ and the average daily air temperature $T_{\mathrm{air}}(d)$ at day d.

The temperature T_h within house h is controlled by the P-controller so that it equals T_{set}. For this, the P-controller sets the mass flow $\dot{m}_h$ through the pump and therefore controls the energy transferred through the heat exchanger to the house.

Each house has a distinct domestic hot water profile generated with the tool *DHWcalc* [16]. It is assumed that the domestic hot water demand of all houses is supplied by the DHN.

2.4.4 District heating network pump

The required pressure difference $\Delta p_{\mathrm{P}}(k) = p^{\mathrm{P}}_{\mathrm{S}}(k) - p^{\mathrm{P}}_{\mathrm{R}}(k)$ at the producer is the difference of the pressure $p^{\mathrm{P}}_{\mathrm{S}}$ at the supply line of the producer and $p^{\mathrm{P}}_{\mathrm{R}}$ at the return line of the producer. The required electric pumping power is given by $P^{\mathrm{pu}}_{\mathrm{el}}(k) = \frac{\dot{m}_{\mathrm{P}}(k) \Delta p_{\mathrm{P}}(k)}{\rho \eta_{\mathrm{pu}}}$ with

the mass flow $\dot{m}_{\mathrm{P}}(k)$ at the producer and $\eta_{\mathrm{pu}} = 0.8$ the efficiency of the pump [17].

2.4.5 Producers

Two different producers are considered. A gas fired combined heat and power unit (CHP) and a LSHP.

The CHP is modeled by the two efficiencies η_{gth} and η_{gtp}. The electric power $\mathrm{P}_{\mathrm{el}}^{\mathrm{CHP}}$, the gas power $\mathrm{P}_{\mathrm{gas}}^{\mathrm{CHP}}$, and the heating power $\dot{\mathrm{Q}}$ are linked by $\mathrm{P}_{\mathrm{el}}^{\mathrm{CHP}} = \eta_{\mathrm{gtp}}\mathrm{P}_{\mathrm{gas}}^{\mathrm{CHP}}$ and $\dot{\mathrm{Q}} = \eta_{\mathrm{gth}}\mathrm{P}_{\mathrm{gas}}^{\mathrm{CHP}}$.

The air source LSHP considered is modeled by a coefficient of performance (COP) [18]

$$\mathrm{COP(k)} = \eta_{\mathrm{C0}}\frac{\mathrm{T_{LSHP}(k)} + \Delta\mathrm{T}}{\mathrm{T_{LSHP}(k)} - \mathrm{T_{air}(k)} + 2\Delta\mathrm{T}}$$

with $\mathrm{T_{LSHP}(k)} = \frac{1}{2}(\mathrm{T_S^P(k)} + \mathrm{T_R^P(k)})$, the supply temperature $\mathrm{T_S^P}$ of the producer, the return temperature $\mathrm{T_R^P}$ of the producer, and the temperature difference $\Delta\mathrm{T} = 10\mathrm{K}$ taking into account the gradient between secondary fluids and refrigerant. The Carnot efficiency factor is set to $\eta_{\mathrm{C0}} = 0.488$ based on the data provided in [19]. The required electric power $\mathrm{P}_{\mathrm{el}}^{\mathrm{LSHP}}(\mathrm{k}) = \dot{\mathrm{Q}}(\mathrm{k})/\mathrm{COP(k)}$ follows.

2.5 Operation of the DHN

The operation of the DHN influences the heat losses, the required pumping power, as well as the efficiency of the LSHP. The supply temperature

$$T_{\mathrm{S}}(k) = \min(\max(u_0 + u_1 T_{\mathrm{air}}(k), T_{\mathrm{S,min}}), T_{\mathrm{S,max}}) \quad (6)$$

is influenced by the two parameters $u_0 \in \mathbb{R}_{>0}$ and $u_1 \in \mathbb{R}_{\leq 0}$ (Fig. 2) with the minimum supply temperature $T_{\mathrm{S,min}} = 60\ °\mathrm{C}$ and the maximum supply temperature $T_{\mathrm{S,max}} = 130\ °\mathrm{C}$. Next to T_{S}, a PI-controller is used for controlling the pressure $p_{\mathrm{S}}^{\mathrm{P}}$. The goal of the PI-controller is to set the difference $p_{\mathrm{S}}^{\mathrm{C}} - p_{\mathrm{R}}^{\mathrm{C}} = 0.1\mathrm{e}^5\ \mathrm{Pa}$ with the supply and return pressure $p_{\mathrm{S}}^{\mathrm{C}}$ and $p_{\mathrm{R}}^{\mathrm{C}}$ of the critical consumer, i.e. the consumer with the longest piping distance to the producer.

3. OPTIMIZATION

The result of each simulation are the required heating powers $\dot{Q}(k)$, the supply and return temperatures $T_{\mathrm{S}}^{\mathrm{P}}(k)$ and $T_{\mathrm{R}}^{\mathrm{P}}(k)$ at the producer, the required electric pumping power $P_{\mathrm{el}}^{\mathrm{pu}}(k)$, and the temperatures $\boldsymbol{T}(k) = [T^1(k) \quad \cdots \quad T^{|H|}(k)]^{\mathrm{T}}$ in the houses at each time-step $k \in K$ with the set of all time-steps K.

3.1 Objective

The objective J of the optimization is to minimize the yearly cost of the DHN consisting of the fuel cost J_{fuel} and the annualized investment cost J_{inv}, i.e.

$$J = J_{\mathrm{fuel}} + J_{\mathrm{inv}}. \quad (7)$$

The investment cost $J_{\mathrm{inv}} = J_{\mathrm{pu}} + J_{\mathrm{pi}} + J_{\mathrm{P}} + J_{\mathrm{H}}$ are comprised of the pump investment cost J_{pu}, the pipe investment cost J_{pi}, the producer investment cost J_{P}, and the house station investment cost J_{H}. Each matter of investment $m \in \{\mathrm{pi, H, P, pu}\}$ is annualized by

$$J_m = \sigma_{\mathrm{debt}} C_m \frac{r}{1-(1+r)^{-w_m}} + \sigma_{\mathrm{equity}}\frac{C_m}{w_m}$$

with the investment cost C_m, the debt ratio $\sigma_{\mathrm{debt}} = 0.29$, the equity ratio $\sigma_{\mathrm{equity}} = 0.71$ [20], and the interest rate $r = 0.04$ [17]. The lifetime w_m of each matter of investment is depicted in Tab. 1.

In each house $h \in H$ a house station has to be constructed. The total investment cost C_{H} for all house stations is given by

$$C_{\mathrm{H}} = \sum_{h \in H} c_{\mathrm{H}}(\dot{Q}_{\mathrm{max}}^h)$$

with the investment cost c_{H} (Tab. 2). The investment cost of the producer depends on the maximum required heating power $\dot{Q}_{\mathrm{max}} = \max_{k \in K} \dot{Q}(k)$ of the DHN and is given by $C_{\mathrm{P}} = c_{\mathrm{P}}(y_{\mathrm{P}}, \dot{Q}_{\mathrm{max}})\dot{Q}_{\mathrm{max}}$, where $c_{\mathrm{P}}(y_{\mathrm{P}}, \dot{Q}_{\mathrm{max}})$ is the specific cost of producer type $y_{\mathrm{P}} \in \{\mathrm{LSHP, CHP}\}$ per unit power. The cost data for both producer types is depicted in Tab. 3. The investment cost of the pump $C_{\mathrm{pu}} = c_{\mathrm{pu}} P_{\mathrm{el,max}}^{\mathrm{pu}}$ depends on the maximum required pumping power $P_{\mathrm{el,max}}^{\mathrm{pu}} = \max_{k \in K} P_{\mathrm{el}}^{\mathrm{pu}}(k)$, where $c_{\mathrm{pu}} = 72\,000\ \mathrm{EUR/MW}$ is the specific investment cost of the pump per unit power [21]. The investment cost C_{pi}^p of pipe p depends on the length l_p and the pipe diameter d_p, which again depends on the choice of y_{S} or y_{R}. The investment cost of all pipes is then given by

$$C_{\mathrm{pi}} = \sum_{p \in E_{\mathrm{S}} \cup E_{\mathrm{R}}} c_{\mathrm{pi}}(d_p) l_p,$$

where $c_{\mathrm{pi}}(d_p)$ is the specific investment cost of pipe p with diameter d_p per unit length. The cost parameters of the considered pipe diameters can be found in Tab. 4. The fuel cost for one year is given by

$$J_{\mathrm{fuel}} = \sum_{k \in K} \Delta t(k)\left[c_{\mathrm{el}}(k)P_{\mathrm{el}}(k) + c_{\mathrm{gas}}P_{\mathrm{gas}}(k)\right]$$

Tab. 1 Lifetime in years [3].

m	w_m
P	20 (LSHP)
P	30 (CHP)
pu	20
pi	40
H	20

Tab. 2 Investment cost of house stations [21].

$\dot{Q}^h_{\max}$ in kW	c_{H} in EUR
≤ 20	6 003
$> 20, \leq 50$	6 353
$> 50, \leq 100$	6 729
> 100	7 438

Tab. 3 Producer cost parameters [21].

type	$\dot{Q}_{\max}$ in MW	c_{P} in EUR/MW
CHP	0.545	890 000
	1.12	720 000
	2.02	730 000
	5.04	660 000
	9.393	650 000
	14.512	650 000
LSHP	1.5	761 000
	5.0	609 000
	20.0	533 000

with the time dependent electric power price $c_{\mathrm{el}}(k)$, the constant gas price c_{gas}, the required gas power $P_{\mathrm{gas}}(k) = P_{\mathrm{gas}}^{\mathrm{CHP}}(k)$ and the required electric power

$$P_{\mathrm{el}}(k) = P_{\mathrm{el}}^{\mathrm{LSHP}}(k) + P_{\mathrm{el}}^{\mathrm{pu}}(k) - P_{\mathrm{el}}^{\mathrm{CHP}}(k).$$

Since *Dymola* uses a variable step size, $\Delta t(k)$ is the step size of time-step k. The gas price is set to $c_{\mathrm{gas}} = 19.4\ \mathrm{EUR/MWh} + 0.201\ \mathrm{t/MWh}\, c_{\mathrm{CO2}}$ with a $\mathrm{CO_2}$ price of $c_{\mathrm{CO2}} = 160\ \mathrm{EUR/t}$, which is the predicted $\mathrm{CO_2}$ price for Germany in the year 2037 [22]. The average c_{el} is $44.49\ \mathrm{EUR/MWh}$ and represents the day ahead auction price for Germany in 2010 [23].

3.2 Constraints

The purpose of a DHN is not fulfilled if the temperature within any connected house is lower than a specified temperature. Therefore, the constraint

$$\min_{k\in K}\left(\min_{h\in H} T_h(k)\right) \geq T_{\min} \qquad (8)$$

is added with the minimum room temperature $T_{\min} = 15°\mathrm{C}$. Since a room temperature of 15°C is not viable for several hours, a second constraint

$$\sum_{k\in K}\begin{cases}\Delta t(k), & \min_{h\in H} T_h(k) < T_{\mathrm{set}} - 1°\mathrm{C} \\ 0, & \text{otherwise}\end{cases} \leq 300\ \mathrm{h} \qquad (9)$$

Is introduced. Equation (9) assures that in not more than $300\ \mathrm{h}$ any room temperature is more than $1\ °\mathrm{C}$ lower than T_{set}. Two constraints are used for assuring a sufficient T_h in each house h, since the time delays within the whole system might lead to deviations from T_{set}.

Tab. 4 Pipe cost parameters. Inner diameters $\mathrm{d_p}$ and heat loss factors $\mathrm{U_p}$ are taken from [25], cost parameters $\mathrm{c_{pi}}$ are approximated based on [21].

d_p in mm	U_p in W/mK	c_{pi} in EUR/m
16.2	0.1128	388
20.4	0.1202	410
26.2	0.1534	490
32.6	0.1596	510
40.8	0.164	540
51.4	0.1863	570
61.4	0.2048	600
73.6	0.22	700
90	0.3246	730
102.2	0.3311	780
114.6	0.3868	850
130.8	0.3188	900

3.3 Optimization algorithm

In order to calculate J, a simulation has to be performed. Therefore, Newton-based optimization algorithms (e.g. interior-point methods or sequential quadratic programming) are not feasible. For minimizing the objective (7), constrained by (8) and (9), a *surrogate* optimization algorithm is used implemented in *Matlab*. Surrogate optimization is designed for time consuming objective functions, e.g. objective functions containing a simulation [24].

4. CASE STUDY

The area of interest is displayed in Fig. 4 with the optimal DHN and the yearly heating demand taken from the heat cadastre. The area of interest is located in an urban area in Hamburg, Germany. Out of 100 houses located in the area with the highest yearly heating demand, 50 were randomly selected. In a first step, a parameter study was conducted by varying all five design values. The results of the parameter study were used to train the surrogate model leading to an optimal design variable configuration.

4.1 Parameter study

The results of the parameter study are depicted in Fig. 5. The yearly heat energy losses

$$\gamma = \frac{\sum_{k\in K}\Delta t(k)[\dot{Q}(k) - \sum_{h\in H}\dot{Q}_h(k)]}{\sum_{k\in K}\Delta t(k)\dot{Q}(k)}\,100\ \%$$

with $\dot{Q}_h$ the heat power demand of house h, vary in the range $2.1\ \%$ and $3.63\ \%$ (Fig. 5(a)). The heat losses γ decrease with an increasing u_0 and a decreasing u_1. For $u_1 < -1.5$ and $u_0 < 90\ °\mathrm{C}$ several simulations failed, since at least one of the constraints (8) and (9) was violated, due to low

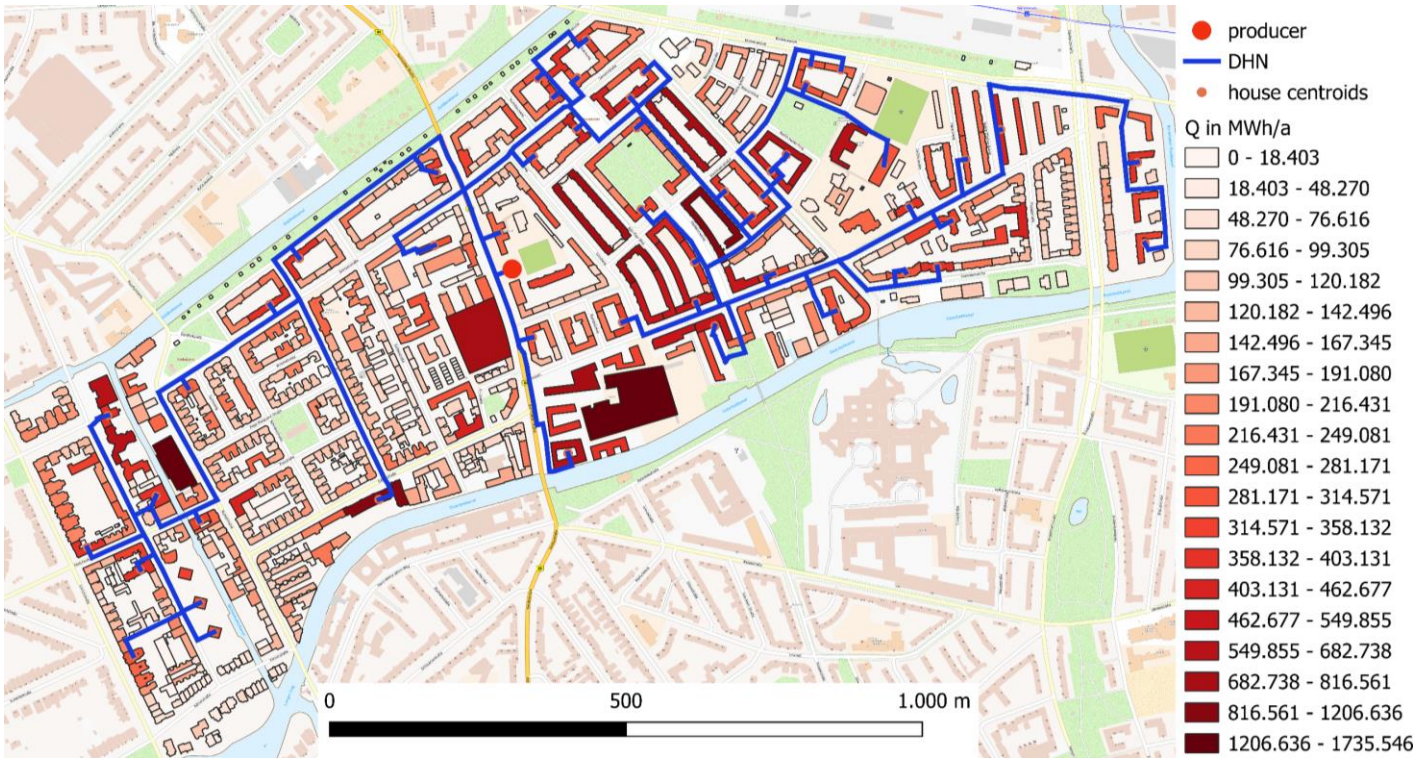

Fig. 4 Area of interest with DHN and yearly heating demand. Map data taken from [26].

supply temperatures. Failed simulations are displayed in Fig. 5(a) by white areas. In contrast to γ, the yearly required electric pumping energy $E_{\mathrm{pu}} = \sum_{k\in K} \Delta t(k) P_{\mathrm{el}}^{\mathrm{pu}}(k)$ increases with a decreasing u_1 and an increasing y_{R} (Fig. 5(b)). Hence, the results concur with the results presented in [5]. Lower supply temperatures and smaller diameters result in lower heat losses but a higher pumping power demand.

The heating power $\dot{Q}$ of the DHN depends on $\dot{m}_{\mathrm{P}}$, $T_{\mathrm{R}}^{\mathrm{P}}$, and $T_{\mathrm{S}}^{\mathrm{P}}$. Due to the mass flow control in the houses, $T_{\mathrm{R}}^{\mathrm{P}}$ is not significantly influenced by the choice of design variables. Therefore, $\dot{Q}_{\max}$ increases mainly with $\dot{m}_{\mathrm{P}}$ and $T_{\mathrm{S}}^{\mathrm{P}}$. The main influence on $\dot{Q}_{\max}$ has the maximum supply temperature $T_{\mathrm{S}}^{\max} = \max_{k\in K} T_{\mathrm{S}}^{\mathrm{P}}(k)$, as depicted in Fig. 6, which again is a result of u_0 and u_1. Fig. 5(c) displays the dependency of $\dot{Q}_{\max}$ on u_1 and y_{S}. The dependency of y_{S} on $\dot{Q}_{\max}$ is only for $y_{\mathrm{S}} < 1\,000\,\mathrm{Pa/m}$ apparent. As y_{S} decreases, $\dot{Q}_{\max}$ increases because larger diameters lead to higher heat losses. With a decreasing u_1, $\dot{Q}_{\max}$ increases and reaches a maximum for $u_1 = -2$. A lower u_1 leads to a more fluctuating $T_{\mathrm{S}}^{\mathrm{P}}$ and in the case of $T_{\mathrm{air}} < 0$ to a higher $\dot{Q}$. After reaching a maximum, $\dot{Q}_{\max}$ decreases with a decreasing u_1. The decreasing $\dot{Q}_{\max}$ for $u_1 < -2$ is a result of limiting $T_{\mathrm{S}}^{\mathrm{P}}$ to a maximum of 130 °C, as can be seen in Fig. 6. For example, choosing $y_{\mathrm{S}} = y_{\mathrm{R}} = 200\,\mathrm{Pa/m}$ leads to a maximum $\dot{Q}_{\max} = 15\,\mathrm{MW}$ ($u_0 = 70\,°\mathrm{C}$, $u_1 = -3$) and a minimum $\dot{Q}_{\max} = 11.38\,\mathrm{MW}$ ($u_0 = 70\,°\mathrm{C}$, $u_1 = 0$). The choice of producer has no influence on $\dot{Q}_{\max}$. Choosing $y_{\mathrm{S}} = y_{\mathrm{R}} = 1\,000\,\mathrm{Pa/m}$ leads to a maximum $\dot{Q}_{\max} = 14.78\,\mathrm{MW}$ ($u_0 = 70\,°\mathrm{C}$, $u_1 = -3$) and a minimum $\dot{Q}_{\max} = 11.91\,\mathrm{MW}$ ($u_0 = 70\,°\mathrm{C}$, $u_1 = 0$). No matter of the choice of y_{S} and y_{R}, a lower $T_{\mathrm{S}}^{\max}$ might result in a higher $\dot{Q}_{\max}$, if $u_1 = -3$, i.e. $T_{\mathrm{S}}^{\mathrm{P}}$ is heavily dependent on T_{air}. This can be explained with energy storing effects within the DHN. The influence of y_{S} and y_{R} on $\dot{Q}_{\max}$ is limited compared with the influence of u_0 and u_1, as can be seen in Fig. 5(c) and Fig. 6.

The yearly cost of the system in the case a LSHP is used varies in the range of $J = 1.9\,\mathrm{mil.\,EUR}$ and $J = 2.08\,\mathrm{mil.\,EUR}$. In the case a CHP is used, the minimum yearly cost is $J = 3.73\,\mathrm{mil.\,EUR}$ and the maximum $J = 3.88\,\mathrm{mil.\,EUR}$. As depicted in Fig. 5(d), in the case of a LSHP, J decreases with a decreasing u_0. This is due to the dependency of the COP of the LSHP on $T_{\mathrm{S}}^{\mathrm{P}}$. In the case a CHP is used, J has a minimum for $u_0 = 100\,°\mathrm{C}$. With a lower u_0, J increases. In contrast to the LSHP, the efficiency of the CHP does not depend on $T_{\mathrm{S}}^{\mathrm{P}}$. However, E_{pu} increases with a decreasing u_0 and with E_{pu}, J_{fuel} increases. For both producer options J decreases with a decreasing y_{S}. This is mainly due to the lower investment cost.

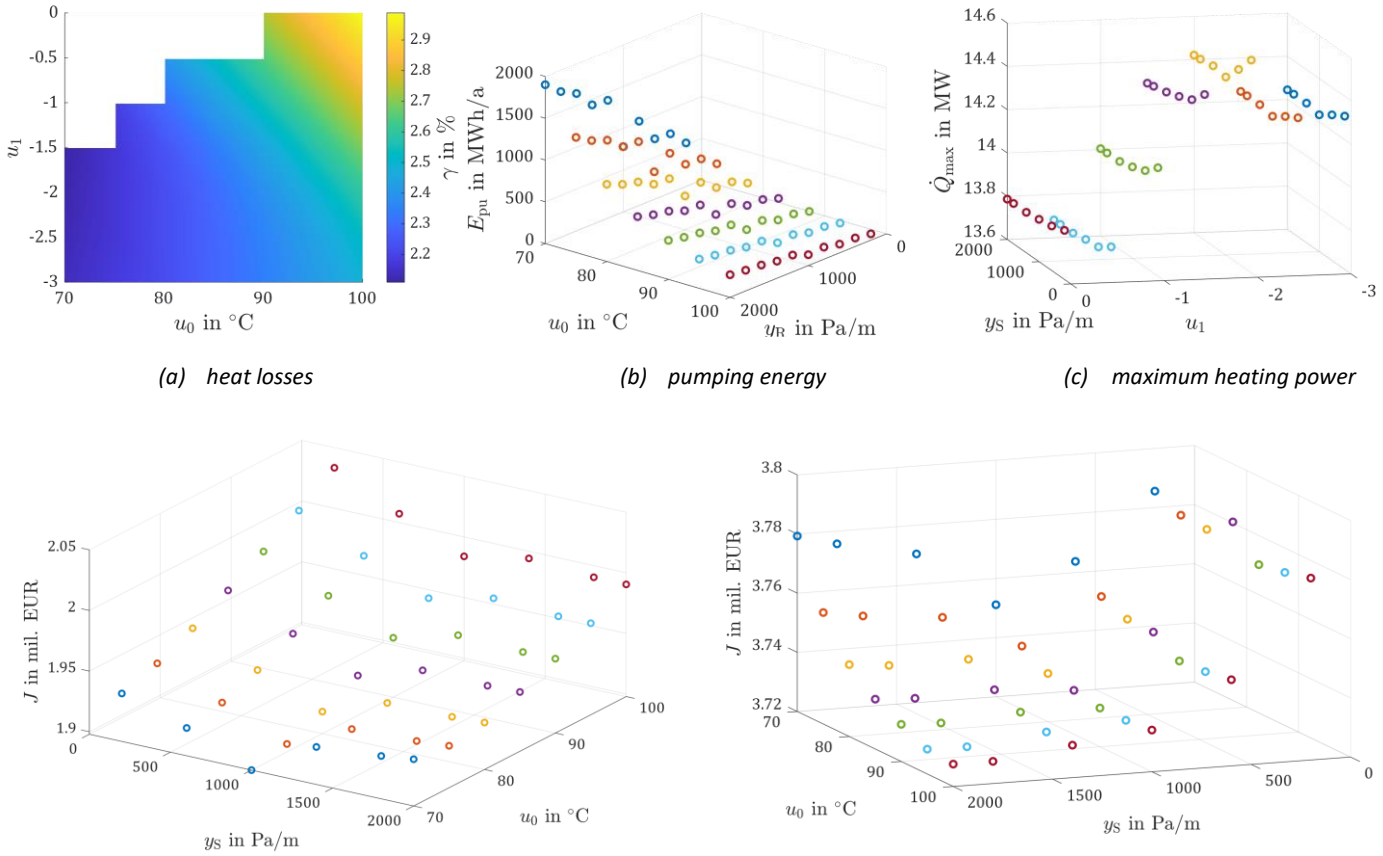

(a) heat losses *(b) pumping energy* *(c) maximum heating power*

(d) objective in the case a LSHP is used *(e) objective in the case a CHP is used*

Fig. 5 Results of the parameter study. In order to plot values that depend on five design values, always the minimum value was selected for the z-axis. For obtaining Fig. (a) the heat losses were interpolated using Matlabs scatteredInterpolant *function using linear interpolation.*

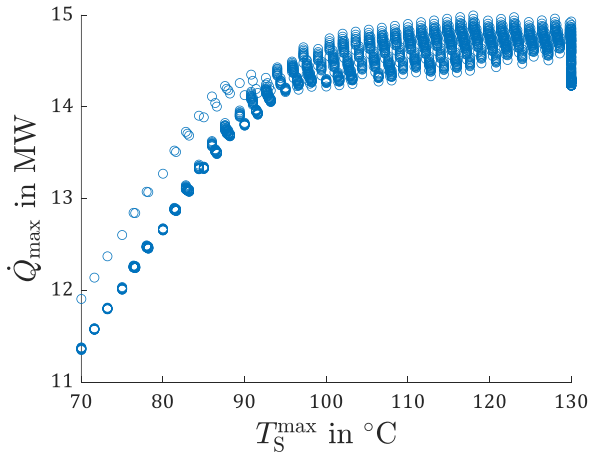

Fig. 6 Maximum required heating power in relation to the maximum supply temperature for each simulation.

4.2 Optimization results

The surrogate optimization results in an optimal design variable configuration of

$$\boldsymbol{z}^* = [1\,000\ \text{Pa/m} \quad 1\,000\ \text{Pa/m} \quad 70\ °\text{C} \quad -1.5 \quad \text{LSHP}]$$

with $J_{\text{inv}}^* = 0.97\ \text{mil. EUR}$ and $J_{\text{fuel}}^* = 0.93\ \text{mil. EUR}$. Although the average J_{inv} is lower for the CHP with $0.79\ \text{mil. EUR}$, the high CO_2 price results in a high J for all design variable configurations where $y_P = \text{CHP}$. The optimizer selects for u_0 the lowest possible value of 70°C. Allowing the optimizer to select lower values for u_0 might result in a lower optimal u_0, since the COP increases with lower supply temperatures. However, with a decreasing u_0, the risk of violated constraints increases (Fig. 5(a)). The optimizer is not selecting lower values for u_1, i.e. a higher influence of T_{air} on T_S^P, since it would result in a higher T_S^{max}. For the optimal design variable configuration, the temperatures at the producer, T_S^P and T_R^P, are depicted in Fig. 7(a). From mid-March to the beginning of November, T_S^P is almost constant at $T_S^P = 60\ °\text{C}$. During the same period, $\dot{m}_P$ is fluctuating in between $0\ \text{kg/s}$ and $70\ \text{kg/s}$. The average COP of the LSHP is 2.82.

In the case a CHP is preferred over a LSHP, the optimal design variable configuration is

$$\boldsymbol{z}_{\text{CHP}}^* = [1\,800\ \text{Pa/m} \quad 1\,800\ \text{Pa/m} \quad 100\ °\text{C} \quad -3 \quad \text{CHP}]$$

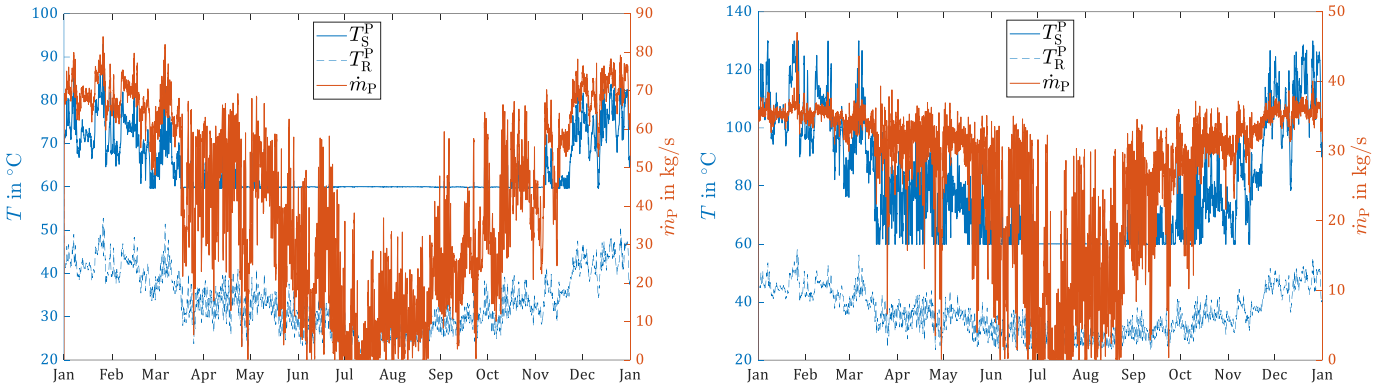

(a) LSHP *(b) CHP*

Fig. 7 Supply and return temperature and mass flow for the optimal design variable configuration for each producer type.

with $J^*_{\mathrm{inv,CHP}} = 0.73\ \mathrm{mil.\,EUR}$ and $J^*_{\mathrm{fuel,CHP}} = 3\ \mathrm{mil.\,EUR}$. Hence, the yearly fuel costs are more than three times higher than the fuel costs in case a LSHP is used. Fig. 7(b) shows T_S^P, T_R^P, and $\dot{m}_P$ for the simulation corresponding to $\boldsymbol{z}^*_{\mathrm{CHP}}$. Due to the low u_1, T_S^P varies in the range of $60\,°\mathrm{C}$ and $130\,°\mathrm{C}$. In comparison with the simulation corresponding to $\boldsymbol{z}^*$, the maximum $\dot{m}_P$ is lower by a factor of approximately two. A result of the overall lower supply temperature T_S^P.

The optimization does not result in larger diameters for the return pipes. The lower pumping power demand, due to smaller diameters, does not compensate for the increase in investment costs and heat losses.

5. DISCUSSION AND CONCLUSION

In this work, a planning method for DHNs is presented. In contrast to traditional planning methods, the operation of the DHN is included in the planning process. The operation is considered by executing a full year simulation within an optimization loop. The execution of one simulation took in between $200\,\mathrm{s}$ and $300\,\mathrm{s}$ for simulating a whole year. The results show that the planning of a DHN highly depends on the assumed prices. Although the investment costs for a CHP are lower than the investment costs for a LSHP, the assumed CO_2 price makes the CHP uneconomic. However, the optimal supply temperature depends on the choice of producer. If a LSHP is selected by the optimizer, the optimal supply temperature varies in between $60\,°\mathrm{C}$ and $85\,°\mathrm{C}$. The sizing of the diameters depends on the choice of producer and the supply temperature. In the case of a CHP and supply temperatures of up to $130\,°\mathrm{C}$, smaller diameters with a TPL of $1\,800\,\mathrm{Pa/m}$ are selected. In the case of a LSHP, due to the lower supply temperature and higher mass flows, the optimizer chooses larger diameters with a TPL of $1\,000\,\mathrm{Pa/m}$.

The simulation time increases with the number of elements (i.e. houses, junctions, and pipes) in the system. In future work, the planning method has to be applied to larger areas. In addition, the presented planning method is constrained to DHNs with a single producer. In order to plan DHNs with more than one producer, the presented method has to be extended.

ACKNOWLEDGEMENT

This research is supported by the German federal ministry of economic affairs and climate action (BMWK) under the agreement no. 03EWR007O2.

REFERENCE

[1] European Commission. (2019). *The European Green Deal*. Communication from the commission (COM(2019) 640 final).

[2] Fraunhofer Institute for Solar Energy Systems ISE. (2021). Wege zu einem klimaneutralen Energiesystem – Update Klimaneutralität 2045.

[3] Lund, H., Möller, B., Mathiesen, B. V., & Dyrelund, A. (2010). The role of district heating in future renewable energy systems. *Energy*, 35(3), 1381–1390. https://doi.org/10.1016/j.energy.2009.11.023

[4] Heendeniya, C. B., Sumper, A., & Eicker, U. (2020). The multi-energy system co-planning of nearly zero-energy districts – Status-quo and future research potential. *Applied Energy*, 267, 114953. https://doi.org/10.1016/j.apenergy.2020.114953

[5] Pirouti, M., Bagdanavicius, A., Ekanayake, J., Wu, J., & Jenkins, N. (2013). Energy consumption and economic analyses of a district heating network. *Energy*, 57, 149–159. https://doi.org/10.1016/j.energy.2013.01.065

[6] Knauer, U., & Knauer, K. (Eds.) (2019). *De Gruyter studies in mathematics: volume 41. Algebraic graph theory: Morphisms, monoids and matrices* (2nd edition). Berlin, Boston: De Gruyter.
[7] Dochev, I., Seller, H., & Peters, I. (2020). Assigning Energetic Archetypes to a Digital Cadastre and Estimating Building Heat Demand. An Example from Hamburg, Germany. *Environmental and Climate Technologies*, 24(1), 233–253. https://doi.org/10.2478/rtuect-2020-0014
[8] Boeing, G. (2024). Modeling and Analyzing Urban Networks and Amenities with OSMnx. Working paper. URL: https://geoffboeing.com/publications/osmnx-paper/
[9] Mehlhorn, K. (1988). A faster approximation algorithm for the Steiner problem in graphs. *Information Processing Letters*, 27(3), 125–128. https://doi.org/10.1016/0020-0190(88)90066-X
[10] Gilbert, E. N., & Pollak, H. O. (1968). Steiner Minimal Trees. *SIAM Journal on Applied Mathematics,* 16(1), 1–29. https://doi.org/10.1137/0116001
[11] Hagberg, A., Swart, P. J., & Schult, D. A. *Exploring network structure, dynamics, and function using NetworkX* (Los Alamos National Laboratory (LANL), Los Alamos, NM (United States) No. LA-UR-08-05495; LA-UR-08-5495).
[12] Cerbe, G., & Lendt, B. (2016). *Grundlagen der Gastechnik* (8th ed.). *Hanser eLibrary*. München: Carl Hanser Verlag GmbH & Co. KG. https://doi.org/10.3139/9783446449664
[13] Hirsch, H., & Nicolai, A. (2022). An efficient numerical solution method for detailed modelling of large 5th generation district heating and cooling networks. *Energy*, 255, 124485. https://doi.org/10.1016/j.energy.2022.124485
[14] Vahlenkamp, T., & Wischhusen, S. (2009). FluidDissipation for Applications - A Library for Modelling of Heat Transfer and Pressure Loss in Energy Systems. In *Linköping Electronic Conference Proceedings, Proceedings of the 7 International Modelica Conference Como, Italy* (pp. 132–141). Linköping University Electronic Press. https://doi.org/10.3384/ecp09430012
[15] DIN Deutsches Institut für Normung e. V. (2021). *Energy efficiency of buildings – Calculation of the net, final and primary energy demand for heating, cooling, ventilation, domestic hot water and lighting*. (DIN/TS, 18599-12).
[16] Jordan, U., Vajen, K. (2005) DHWcalc: Program to generate Domestic Hot Water Profiles with Statistical Means for User Defined Conditions. In *Proceedings of the ISES Solar World Congress, Orlando, 8. - 12.8.2005.*
[17] Hering, D., Xhonneux, A., & Müller, D. (2021). Design optimization of a heating network with multiple heat pumps using mixed integer quadratically constrained programming. *Energy*, 226, 120384. https://doi.org/10.1016/j.energy.2021.120384
[18] Speerforck, A., Ling, J., Aute, V., Radermacher, R., & Schmitz, G. (2017). Modeling and simulation of a desiccant assisted solar and geothermal air conditioning system. *Energy*, 141, 2321–2336. https://doi.org/10.1016/j.energy.2017.11.151
[19] Jesper, M., Schlosser, F., Pag, F., Walmsley, T. G., Schmitt, B., & Vajen, K. (2021). Large-scale heat pumps: Uptake and performance modelling of market-available devices. *Renewable and Sustainable Energy Reviews*, 137, 110646. https://doi.org/10.1016/j.rser.2020.110646
[20] Oliva H., S., & Garcia G., M. (2023). Investigating the impact of variable energy prices and renewable generation on the annualized cost of hydrogen. *International Journal of Hydrogen Energy*, *48*(37), 13756–13766.
https://doi.org/10.1016/j.ijhydene.2022.12.304
[21] Ministry of the Environment, Climate Protection and the Energy Sector Baden-Württemberg (2023). *Kommunale Wärmeplanung Einführung in den Technikkatalog.*
[22] 50Hertz Transmission GmbH, Amprion GmbH, TenneT TSO GmbH, & TransnetBW GmbH (2023). *Netzentwicklungsplan Strom 2037 mit Ausblick 2045: Erster Entwurf der Übertragungsnetzbetreiber.*
[23] Energy-Charts, Electricity production and spot prices in Germany in 2010. URL: https://energy-charts.info/charts/, accessed: 2024-08-14.
price spot market/chart.htm?l=en&c=DE, accessed: 2023-06-13.
[24] Queipo, N. V., Haftka, R. T., Shyy, W., Goel, T., Vaidyanathan, R., & Kevin Tucker, P. (2005). Surrogate-based analysis and optimization. *Progress in Aerospace Sciences*, 41(1), 1–28. https://doi.org/10.1016/j.paerosci.2005.02.001
[25] REHAU GmbH (2020). *Technische Information – Vorisolierte REHAU Systeme für die Wärme- & Kälteversorgung*. Retrieved from https://www.rehau.com/downloads/174412/insulpex-nah-und-fernwaermesystem.pdf
[26] Bundesamt für Kartographie und Geodäsie (2024). https://sgx.geodatenzentrum.de/web_public/Datenquellen_TopPlus_Open.pdf